JACS
JOURNAL OF THE AMERICAN CHEMICAL SOCIETY
Communication
pubs.acs.org/JACS

Segregated and Alternately Stacked Donor/Acceptor Nanodomains in Tubular Morphology Tailored with Zinc Porphyrin–C_{60} Amphiphilic Dyads: Clear Geometrical Effects on Photoconduction

Richard Charvet,*[,†,○] Yohei Yamamoto,*[,†,‡] Takayuki Sasaki,[‡] Jungeun Kim,[§] Kenichi Kato,[#,∥] Masaki Takata,[§,∥] Akinori Saeki,[#] Shu Seki,[#] and Takuzo Aida*[,†,⊥]

[†]ERATO–SORST Nanospace Project, Japan Science and Technology Agency (JST), 2-3-6 Aomi, Koto-ku, Tokyo 135-0064, Japan

[‡]Division of Materials Science and Tsukuba Research Center for Interdisciplinary Materials Science (TIMS), Faculty of Pure and Applied Sciences, University of Tsukuba, 1-1-1 Tennodai, Tsukuba, Ibaraki 305-8573, Japan

[§]Japan Synchrotron Radiation Research Institute (JASRI), 1-1-1 Kouto, Sayo-cho, Sayo-gun, Hyogo 679-5198, Japan

[∥]RIKEN SPring-8 Center, 1-1-1 Kouto, Sayo-cho, Sayo-gun, Hyogo 679-5148, Japan

[#]Graduate School of Engineering, Osaka University, 2-1 Yamadaoka, Suita, Osaka 565-0871, Japan

[⊥]Department of Chemistry and Biotechnology, School of Engineering, The University of Tokyo, 7-3-1 Hongo, Bunkyo-ku, Tokyo 113-8656, Japan

Supporting Information

ABSTRACT: Amphiphilic zinc porphyrin (P_{Zn}; electron donor, D)–fullerene (C_{60}; electron acceptor, A) dyads **2** and **3**, bearing an identical hydrophilic wedge with triethylene glycol chains but different linkers between the P_{Zn} and C_{60} units, self-assemble into nanotubes with essentially different dimensional and geometrical features from one another. The nanotube from dyad **2** with an ester linker consists of a bilayer wall formed with coaxially segregated D and A nanodomains along the tube axis (coaxial D–A heterojunction), thereby displaying explicit photoconductivity with ambipolar carrier transport properties. In contrast, the nanotube from dyad **3** with a rigid arylacetylene linker consists of a monolayer wall with an alternate geometry of D/A stacking, resulting in poor photoconducting outputs. Such a geometrical difference also significantly affects the photovoltaic properties.

Tailoring electron donor (D)–acceptor (A) heterojunctions is one of the most essential subjects in the design of optoelectronic materials for photon–energy conversion.[1] In particular, for the development of high-performance solution-processable photovoltaic cells, rational molecular assembling strategies are needed to construct segregated D and A domains for transporting holes and electrons, respectively. Furthermore, such segregated D and A domains should be connected together at a wider interface, preferably with nanoscale precision, for a better photoinduced charge-separation efficiency.[2] Although utilization of so-called 'bulk D–A heterojunctions' may be a practical solution for device fabrication, such structures are hard to elaborate because they are formed just coincidentally by phase separation of D and A components. Moreover, D and A tend to form a charge-transfer (CT) complex, which often hampers photovoltaic outputs. In this context, the use of D–A dyads, if properly designed, may provide a rational synthetic strategy for nanoscale D–A heterojunctions.[3] In fact, we succeeded in tailoring elaborate D–A heterojunctions in fibrous[4] and tubular[5] morphologies and also in liquid crystals[6] using strategically designed D–A dyads. Successful examples so far reported by our group feature hexabenzocoronene and oligothiophene as D components, which are combined with trinitrofluorenone, fullerene, and perylenediimide as electron acceptors.[4–6] Some of the resultant assemblies indeed displayed remarkable photoconductive and even photovoltaic outputs.[5a–c,6] However, their absorption coefficients for visible light are not satisfactorily large. Therefore, we newly focused on porphyrin derivatives as the donor components and designed amphiphilic porphyrin–fullerene (C_{60}) dyad **1** (Figure 1). As reported previously, this compound self-assembles into photoconducting nanofibers with a core–shell A–D heterojunction.[7] However, such an ideal one-dimensional (1D) nanostructure develops only when dyad **1** is enantiomerically pure with respect to the chiral fullerene unit. In contrast, its racemate self-assembles into spheres. Obviously, the molecular design involving optical resolution is tedious and not practical in view of device applications.

Here we report newly designed zinc porphyrin (P_{Zn})–C_{60} dyads **2** and **3** (Figure 1), which self-assemble into discrete 1D nanostructures. Although dyads **1**–**3** differ from one another in their linker parts for connecting the porphyrin and C_{60} units, the nanostructures from dyads **2** and **3** are both tubules (Figure 4) rather than solid fibers. As highlighted in this communication, these nanotubes possess completely different D/A geometries from each other. The nanotube from **2** consists of a bilayer wall featuring coaxially segregated D and A domains along the tube axis (Figure 4a). In sharp contrast, the nanotube from **3** is composed of a monolayer wall with an alternate geometry of D/A stacking (Figure 4b). Noteworthy, the former nanotube displays much better photoconduction profiles and photovoltaic outputs than the latter.

Received: December 4, 2011
Published: January 25, 2012

 © 2012 American Chemical Society

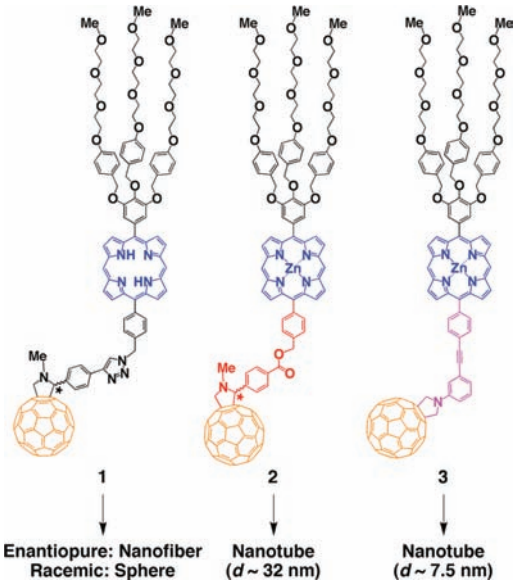

Figure 1. Molecular structures of dyads **1**−**3** and resultant nanostructures upon self-assembly. *d* indicates nanotube diameters.

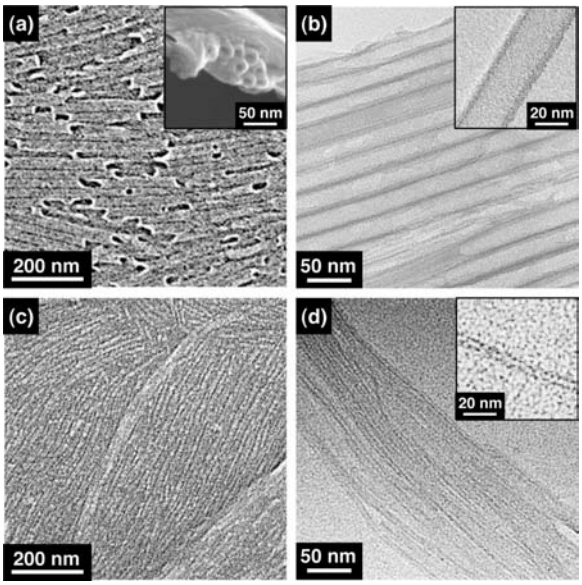

Figure 2. (a, c) SEM and (b, d) TEM micrographs of air-dried suspensions of tubularly assembled **2** (a, b) and **3** (c, d).

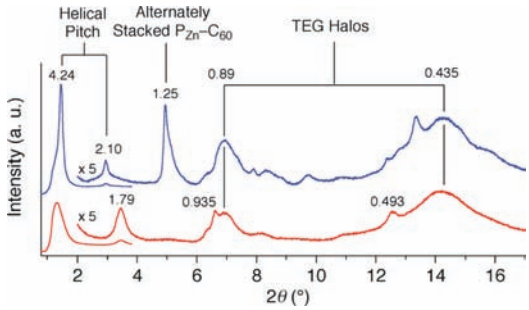

Figure 3. XRD patterns of tubularly assembled **2** (red) and **3** (blue). Numerical values indicate *d*-spacings (nm).

Dyads **2** and **3** were synthesized and unambiguously characterized as described in the Supporting Information.[8] Electronic absorption spectroscopy of a toluene solution of **2** displayed a Soret band and Q-band of the P_{Zn} unit at 414 and 544 nm, respectively (Figure S1a, black).[8] Differential pulse voltammetry (DPV) of its CH_2Cl_2 solution showed two reduction and multiple oxidation peaks (Figure S2a).[8] From the offsets of the redox peaks and absorption edges of the P_{Zn} and C_{60} units, the energy levels of each chromophore in dyad **2** were determined as shown in Figure S2b.[8] Apparently, the P_{Zn}-to-C_{60} photoinduced electron transfer (PET) is energetically allowed. In fact, most (85−90%) of the fluorescence of **2** from its P_{Zn} unit was quenched (Figure S3).[8] The same holds true for dyad **3** (Figure S3).[8]

Upon addition of MeOH, a toluene solution of **2** displayed a marked color change from pink to pale orange when the MeOH content in the medium reached 65% in volume ([**2**] = 4 × 10^{-5} M, Figure S1a, inset).[8] When allowed to stand overnight at 25 °C, the resulting solution turned into an orange-red-colored suspension (Figure S1a, inset).[8] Of interest, in ∼4 h after the addition of MeOH, the Soret absorption band at 414 nm fell off abruptly, affording a new absorption band at 441 nm with a shoulder at 400 nm (Figure S1a and S1b).[8] The spectral change thus observed is typical of *J*-aggregated zinc porphyrins.[9] Scanning (SEM; Figure 2a) and transmission (TEM; Figure 2b) electron micrographs of an air-dried suspension allowed us to confirm the formation of nanotubes[5] with a uniform diameter and wall thickness of 32 and 5.5 nm, respectively. Considering the edge-to-edge distance between the P_{Zn} and C_{60} units in **2** (∼3.2 nm when extended), the nanotubular wall most likely adopts a bilayer configuration. The nanotube displayed electron diffractions (EDs) with a periodicity of 0.51 nm (Figure S4),[8] which is assignable to the stacking distance of the *J*-aggregated P_{Zn} units. Furthermore, X-ray diffraction (XRD) analysis (Figure 3, red) showed a set of three distinct peaks with 2θ = 3.45°, 6.62°, and 12.6° (*d*-spacings: 1.79, 0.935, and 0.493 nm, respectively), along with broad halos (2θ = 7° and 14°) by scattering of the TEG domain. Since such sharp diffractions are likely caused by Zn^{2+}, the P_{Zn} units in the nanotubular wall are placed periodically. Therefore, we conclude that the nanotube adopts a coaxial D/A configuration, where an inner tubular domain, composed of clustered C_{60} units (A), is laminated on both of its sides by a molecular layer of *J*-aggregated P_{Zn} units (Figure 4a). Consequently, the hydrophilic TEG chains cover both the inner and outer surfaces of the nanotube. In fact, a water droplet on a cast film of the nanotubes showed a contact angle of 32° (Figure S5a),[8] which is far smaller than that on a film sample cast from a CH_2Cl_2 solution of nonassembled **2** (64°, Figure S5b).[8]

As described previously, dyad **3**, when allowed to assemble in toluene/MeOH, likewise afforded nanotubules. However, judging from the SEM (Figure 2c) and TEM (Figure 2d) micrographs, the tube diameter (d = 7−8 nm) and wall thickness (t = 1.7−1.8 nm) are much smaller than those of nanotubularly assembled **2** (*vide ante*, d = 32 nm, t = 5.5 nm). Note that the wall thickness thus estimated is even smaller than the edge-to-edge distance between the P_{Zn} and C_{60} units in **3** (∼3.2 nm), suggesting that the nanotubular wall is a monolayer, where the dyad most likely adopts a tilted orientation relative to the radial direction of the nanotube (Figure 4b). Suppose that the TEG chains of **3** prefer to be exposed to the polar medium (toluene/MeOH) as in the case of the assembly of **2** (*vide ante*), the P_{Zn} and C_{60} units in the nanotube from **3** likely stack with an alternate geometry (Figure 4b). Accordingly, XRD

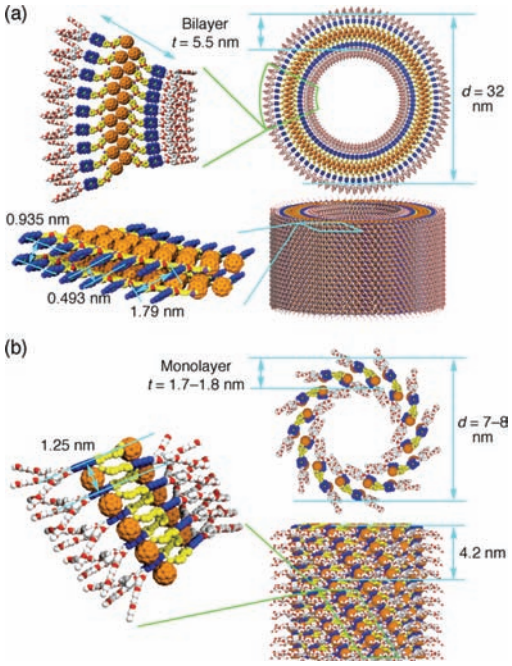

Figure 4. Schematic representations of tubularly assembled **2** (a) and **3** (b). Blue-, orange-, and yellow-colored parts represent P_{Zn}, C_{60}, and linker units, respectively, while chains drawn with red and white spheres denote triethylene glycol (TEG) chains. *d* and *t* indicate nanotube diameters and wall thicknesses.

analysis of tubularly assembled **3** displayed a characteristic diffraction with $2\theta = 4.95°$ (*d*-spacing: 1.25 nm; Figure 3, blue), which is assignable to the distance between the P_{Zn} units that sandwich C_{60}.[10] In relation to this observation, tubularly assembled **3** in toluene/MeOH showed a weak and broad absorption tail centered at 700 nm (Figure S6a, inset),[8] which is assignable to a CT absorption band typically observed for zinc porphyrins upon complexation with fullerenes.[10,11] Of interest, two X-ray diffraction peaks in a small-angle region at $2\theta = 1.46°$ and 2.95° (*d*-spacings: 4.24 and 2.10 nm, respectively; Figure 3, blue) suggest that the P_{Zn}–C_{60} units upon alternate stacking in the nanotube form a helically twisted array (Figure 4b).

Due to the coexistence of the electron donor (P_{Zn}) and acceptor (C_{60}) units, the nanotubes from **2** and **3** were both photoconductive. However, their performances obviously differed from one another. Figure 5a shows current–voltage (*I*–*V*) profiles of cast films of tubularly assembled **2** (red) and **3** (blue) upon photoirradiation (λ = 300–650 nm), where the former nanotube, featuring the coaxially segregated P_{Zn}–C_{60} heterojunction, displayed a much larger photocurrent than the latter adopting the alternate geometry of P_{Zn}/C_{60} stacking. As also shown in Figure 5a (inset), the photocurrent switching of tubularly assembled **2** was prompt and repeatable by turning on and off the light. When this coaxial D–A heterojunction nanotube was exposed to a pulsed laser at 355 nm, charge carriers were generated, whose time-resolved microwave conductivity[12] (TRMC, $\phi\Sigma\mu_{max} = 1.02 \times 10^{-3}$ cm^2 V^{-1} s^{-1}) was 6.5 times greater than that of the nanotube from **3** ($\phi\Sigma\mu_{max} = 0.16 \times 10^{-3}$ cm^2 V^{-1} s^{-1}) (Figure 5b). The photocurrent action spectrum of the nanotube from **2** was in good agreement with its absorption spectral profile (Figure 5c), indicating that the photocurrent, as also expected from the P_{Zn} fluorescence quenching (*vide ante*, Figure S3),[8] is generated mainly by an electron transfer from the photoexcited P_{Zn} species to the C_{60}

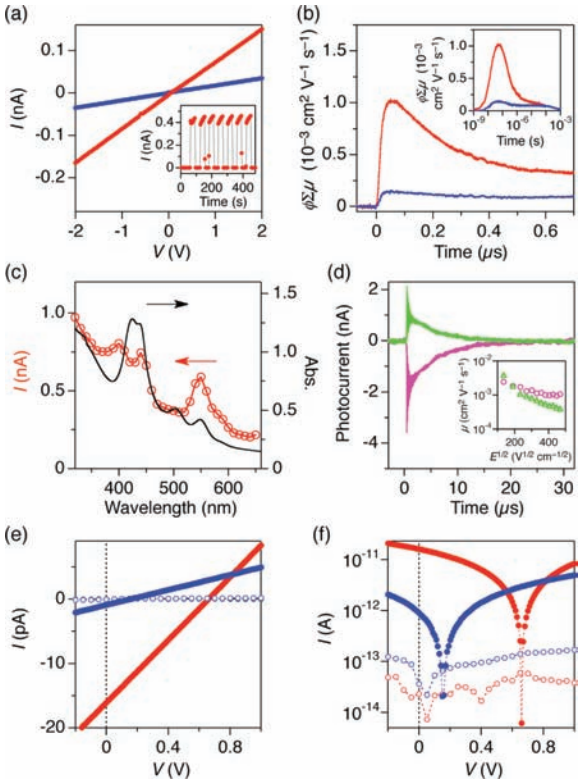

Figure 5. (a) *I*–*V* profiles at 25 °C of cast films of nanotubularly assembled **2** (red) and **3** (blue) on Au electrodes upon photoirradiation (λ = 300–650 nm). Inset: A change in electric current at 25 °C of a cast film of tubularly assembled **2** upon turning on and off the light. (b) TRMC profiles at 25 °C of cast films of tubularly assembled **2** (red) and **3** (blue) upon irradiation by a pulsed laser at 355 nm. Inset shows TRMC profiles acquired in a longer time scale. (c) Photocurrent action spectrum (red) and electronic absorption spectrum (black) at 25 °C of a cast film of tubularly assembled **2**. (d) Time-of-flight (TOF) transient photocurrent profiles at 25 °C of a cast film of tubularly assembled **2** for hole (green) and electron (pink) under E-fields of -1.27×10^5 and $+1.27 \times 10^5$ V cm^{-1}, respectively, upon irradiation by a pulsed laser at 355 nm. Inset shows hole (green) and electron (pink) mobilities as a function of applied E-field. (e, f) *I*–*V* (e) and log *I*–*V* (f) profiles at 25 °C of cast films of tubularly assembled **2** (red) and **3** (blue) in PV devices in the dark (open circles) and upon photoirradiation (closed circles, light power density; 46 mW cm^{-2}).

unit. Of particular interest, time-of-flight (TOF) photoconductivity measurements indicated that tubularly assembled **2** is ambipolar and capable of transporting both holes and electrons (Figure 5d). When the magnitude of an applied electric field (E-field) was changed, the hole (μ_h) and electron (μ_e) mobilities were varied (Figure 5d, inset), but they remained rather comparable to each other over a wide E-field range. For example, at an E-field of 0.36×10^5 V m^{-1}, μ_h and μ_e became identical to one another ($\sim 1.8 \times 10^{-3}$ cm^2 V^{-1} s^{-1}).

Such an ambipolar charge transport character with well-balanced μ_h and μ_e is important for photovoltaic (PV) outputs.[5c] In fact, tubularly assembled **2** shows a photovoltaic response. For this study, a conventional top-contact device configuration was not applicable because the nanotube upon drop casting did not form a pinhole-free homogeneous film. Instead, we employed a particular device configuration (Figure S7)[5c,8] analogous to field-effect transistors, where film samples were allowed to bridge two different electrodes horizontally.

Thus, a nanotube suspension was cast onto a fluoroalkyl-coated glass substrate, prepatterned with PEDOT:PSS/Au/Ti [PEDOT, poly(3,4-ethylenedioxythiophene); PSS, poly-(styrenesulfonate)] and TiO_x/Ti/Al electrodes with an 8−15 μm separation.[8] Upon exposure to light with a power density of 46 mW cm^{-2} from the back side of the glass substrate, the film sample displayed a PV response with an open-circuit voltage (V_{OC}) and a short-circuit current (I_{SC}) of 0.66 V and 16 pA, respectively (Figure 5e and 5f, red). I_{SC} was switched promptly and repeatedly upon turning on and off the light with an on/off current ratio greater than 10^3 (Figure S8a, red).[8] In sharp contrast, a cast film of the nanotube of **3**, likewise integrated into the same device configuration, exhibited a very poor PV response with V_{OC} and I_{SC} values of only 0.16 V and 0.9 pA, respectively (Figure 5e and 5f, blue). I_{SC} and V_{OC} were enhanced by increasing the light intensity (Figure S8b and S8c, respectively)[8] but much less so than the case of **2** having a segregated D−A stacking. Although the device configuration employed here is not appropriate for evaluating the power conversion efficiencies, it is now clear that the nanotube of **2** is superior to that of **3** for PV applications.

In conclusion, we developed P_{Zn}−C_{60} nanotubes with segregated and alternately stacked donor (D; P_{Zn})/acceptor (A; C_{60}) configurations and demonstrated clear geometrical effects on optoelectronic outputs. The nanotube from **2** with a coaxial D−A heterojunction along the tube axis (Figure 4a) displays much better photoconducting properties than that from **3** with an alternate D/A stacking geometry (Figure 4b). Together with its explicit ambipolar carrier transport character, the PV output of the former nanotube is superior to the latter. The results presented here contribute to the progress of bottom-up nanoscale organic electronics.

■ ASSOCIATED CONTENT

Supporting Information

Details of synthesis, self-assembly, MALDI-TOF mass spectra, NMR spectra, electronic absorption spectra, DPV, contact angles, fluorescence spectra, SEM, TEM, ED, and PV data. This material is available free of charge via the Internet at http://pubs.acs.org.

■ AUTHOR INFORMATION

Corresponding Author

racharvet@yahoo.com; yamamoto@ims.tsukuba.ac.jp; aida@macro.t.u-tokyo.ac.jp

Present Address

○ADOCIA, 115 avenue Lacassagne, 69003 Lyon, France.

Notes

The authors declare no competing financial interest.

■ ACKNOWLEDGMENTS

The synchrotron radiation experiments were performed at BL02B2 and BL44B2 in SPring-8 with the approval of JASRI (Proposal Nos. 2008A1644 and 2008B1777, the Priority Nanotechnology Support Program) and RIKEN (Proposal No. 20100024), respectively. This work was partly supported by a Grant-in-Aid for Young Scientist B (23750144) from the Ministry of Education, Culture, Sports, Science and Technology, Japan, and Kato Science Foundation (H23_2006).

■ REFERENCES

(1) (a) Schmidt-Mende, L.; Fechtenkötter, A.; Müllen, K.; Moons, E.; Friend, R. H.; MacKenzie, J. D. *Science* **2001**, *293*, 1119−1122. (b) Kim, Y.; Cook, S.; Tuladhar, S. M.; Choulis, S. A.; Nelson, J.; Durrant, J. R.; Bradley, D. D. C.; Giles, M.; Mcculloch, I.; Ha, C.-S.; Ree, M. *Nat. Mater.* **2006**, *5*, 197−203. (c) Huang, Y.-S.; Westenhoff, S.; Avilov, I.; Sreearunothai, P.; Hodgkiss, J. M.; Deleener, C.; Friend, R. H.; Beljonne, D. *Nat. Mater.* **2008**, *7*, 483−489. (d) Beaujuge, P. M.; Fréchet, J. M. J. *J. Am. Chem. Soc.* **2011**, *133*, 20009−20029.

(2) (a) Günes, S.; Neugebauer, H.; Sariciftci, N. S. *Chem. Rev.* **2007**, *107*, 1324−1338. (b) Thompson, B. C.; Fréchet, J. M. J. *Angew. Chem., Int. Ed.* **2008**, *47*, 58−77. (c) Pisula, W.; Kastler, M.; Wasserfallen, D.; Robertson, J. W. F.; Nolde, F.; Kohl, C.; Müllen, K. *Angew. Chem., Int. Ed.* **2006**, *45*, 819−823. (d) Wei, Z.; Jin, W.; Fukushima, T.; Saeki, A.; Seki, S.; Aida, T. *Science* **2011**, *334*, 340−343.

(3) (a) van der Boom, T.; Hayes, R. T.; Zhao, R. T.; Bushard, P. J.; Weiss, E. A.; Wasielewski, M. R. *J. Am. Chem. Soc.* **2002**, *124*, 9582−9590. (b) Georgakilas, V.; Pellarini, F.; Prato, M.; Guldi, D. M.; Melle-Franco, M.; Zerbetto, F. *Proc. Natl. Acad. Sci. U.S.A.* **2002**, *99*, 5075−5080. (c) Neuteboom, E. E.; Maskers, S. C. J.; van Hal, P. A.; van Duren, J. K. J.; Meijer, E. W.; Janssen, R. A.; Dupin, H.; Pourtois, G.; Cornil, J.; Lazzaroni, R.; Brédas, J.-L.; Beljonne, D. *J. Am. Chem. Soc.* **2003**, *125*, 8625−8638. (d) Beckers, E.; Maskers, S. C. J.; Schenning, A. P. H. J.; Chen, Z.; Würthner, F.; Marsal, P.; Beljonne, D.; Cornil, J.; Janssen, R. A. J. *J. Am. Chem. Soc.* **2006**, *128*, 649−657. (e) Sisson, A. L.; Sakai, N.; Banerji, N.; Fürstenberg, A.; Vauthey, E.; Matile, S. *Angew. Chem., Int. Ed.* **2008**, *47*, 3727−3729. (f) Kira, A.; Umeyama, T.; Matano, Y.; Yoshida, K.; Isoda, S.; Park, J. K.; Kim, D.; Imahori, H. *J. Am. Chem. Soc.* **2009**, *131*, 3198−3200. (g) Tu, S.; Kim, S. H.; Joseph, J.; Modarelli, D. A.; Parquette, J. R. *J. Am. Chem. Soc.* **2011**, *133*, 19125−19130.

(4) Li, W.-S.; Saeki, A.; Yamamoto, Y.; Fukushima, T.; Seki, S.; Ishii, N.; Kato, K.; Takata, M.; Aida, T. *Chem.—Asian J.* **2010**, *5*, 1566−1572.

(5) (a) Yamamoto, Y.; Fukushima, T.; Suna, Y.; Ishii, N.; Saeki, A.; Seki, S.; Tagawa, S.; Taniguchi, M.; Kawai, T.; Aida, T. *Science* **2006**, *314*, 1761−1764. (b) Yamamoto, Y.; Fukushima, T.; Saeki, A.; Seki, S.; Tagawa, S.; Ishii, N.; Aida, T. *J. Am. Chem. Soc.* **2007**, *129*, 9276−9277. (c) Yamamoto, Y.; Zhang, G.; Jin, W.; Fukushima, T.; Ishii, N.; Saeki, A.; Seki, S.; Tagawa, S.; Minari, T.; Tsukagoshi, K.; Aida, T. *Proc. Natl. Acad. Sci. U.S.A.* **2009**, *106*, 21051−21056. (d) He, Y.; Yamamoto, Y.; Jin, W.; Fukushima, T.; Saeki, A.; Seki, S.; Ishii, N.; Aida, T. *Adv. Mater.* **2010**, *22*, 829−832. (e) Saeki, A.; Yamamoto, Y.; Koizumi, Y.; Fukushima, T.; Aida, T.; Seki, S. *J. Phys. Chem. Lett.* **2011**, *2*, 2549−2554.

(6) Li, W.-S.; Yamamoto, Y.; Fukushima, T.; Saeki, A.; Seki, S.; Tagawa, S.; Masunaga, H.; Sasaki, S.; Takata, M.; Aida, T. *J. Am. Chem. Soc.* **2008**, *130*, 8886−8887.

(7) Hizume, Y.; Tashiro, K.; Charvet, R.; Yamamoto, Y.; Saeki, A.; Seki, S.; Aida, T. *J. Am. Chem. Soc.* **2010**, *132*, 6628−6629.

(8) See Supporting Information.

(9) (a) Okada, S.; Segawa, H. *J. Am. Chem. Soc.* **2003**, *125*, 2792−2796. (b) Yamaguchi, T.; Kimura, T.; Matsuda, H.; Aida, T. *Angew. Chem., Int. Ed.* **2004**, *43*, 6350−6355. (c) Sakata, A.; Kobuke, Y. *Org. Biomol. Chem.* **2007**, *5*, 1679−1691. (d) Tsuda, A.; Alam, Md. A.; Harada, T.; Yamaguchi, T.; Ishii, N.; Aida, T. *Angew. Chem., Int. Ed.* **2007**, *46*, 8918−8202.

(10) Zheng, J.-Y.; Tashiro, K.; Hirabayashi, Y.; Kinbara, K.; Saigo, K.; Aida, T.; Sakamoto, S.; Yamaguchi, K. *Angew. Chem., Int. Ed.* **2001**, *40*, 1858−1861.

(11) (a) Armaroli, N.; Marconi, G.; Echegoyen, L.; Bourgeois, J.-P.; Diedrich, F. *Chem.—Eur. J.* **2000**, *6*, 1629−1645. (b) Charvet, R.; Jiang, D.-L.; Aida, T. *Chem. Commun.* **2004**, 2664−2665. (c) Imahori, H.; Ueda, M.; Kang, S.; Hayashi, S.; Kaji, H.; Seki, S.; Saeki, A.; Tagawa, S.; Umeyama, T.; Matano, Y.; Yoshida, K.; Isoda, S.; Shiro, M.; Tkachenko, N. V.; Lemmetyinen, H. *Chem.—Eur. J.* **2007**, *13*, 10182−10193.

(12) Saeki, A.; Seki, S.; Takenobu, T.; Iwasa, Y.; Tagawa, S. *Adv. Mater.* **2008**, *20*, 920−923.